Microporous and Mesoporous Materials 255 (2018) 76–83

Contents lists available at ScienceDirect

Microporous and Mesoporous Materials

journal homepage: www.elsevier.com/locate/micromeso

Facile synthesis of triazine-triphenylamine-based microporous covalent polymer adsorbent for flue gas CO_2 capture

Swapan K. Das, Xinbo Wang, Zhiping Lai*

Advanced Membrane and Porous Materials Center, Chemical and Biological Engineering, Division of Physical Science and Engineering, King Abdullah University of Science and Technology (KAUST), Thuwal, 23955-6900, Saudi Arabia

ARTICLE INFO

Article history:
Received 1 December 2016
Received in revised form
15 April 2017
Accepted 15 July 2017
Available online 17 July 2017

Keywords:
Covalent porous polymer
CO_2 capture
Microporous
Flue gas
Gas adsorption

ABSTRACT

The sustainable capture and sequestration of CO_2 from flue gas emission is an important and unavoidable challenge to control greenhouse gas release and climate change. In this report, we describe a triazine-triphenylamine-based microporous covalent organic polymer under mild synthetic conditions. ^{13}C and ^{15}N solid-state NMR and FTIR analyses confirm the linkage of the triazine and triphenylamine components in the porous polymer skeleton. The material is composed of spherical particles 1.0 to 2.0 μm in size and possesses a high surface area (1104 m^2/g). The material exhibits superb chemical robustness under acidic and basic conditions and high thermal stability. Single-component gas adsorption exhibits an enhanced CO_2 uptake of 3.12 mmol/g coupled with high sorption selectivity for CO_2/N_2 of 64 at 273 K and 1 bar, whereas the binary gas mixture breakthrough study using a model flue gas composition at 298 K shows a high CO_2/N_2 selectivity of 58. The enhanced performance is attributed to the high Lewis basicity of the framework, as it favors the interaction with CO_2.

1. Introduction

Over the past several decades, significant research effort has been devoted to carbon capture and sequestration (CCS) due to widespread concerns of the rapid increase in the CO_2 level in the atmosphere, which creates adverse effects such as global climate change and ocean acidification [1–5]. Aqueous amine scrubbing is a commercialized CO_2 capture process, but it is corrosive and energy intensive and thus economically unfeasible for large-scale CCS applications [6,7]. To date, various CCS technologies have been developed, such as cryogenic distillation, membrane separation and adsorption [4]. Adsorption by porous solid adsorbents (PSAs) has been proposed as one of the most feasible alternatives [7–9]. The process, in principle, incurs a lower energy penalty than amine scrubbing, but the synthesis of high-performance PSAs that meet all practical requirements remains a large challenge [8,10]. A number of porous materials are under intensive investigation, including activated carbons [11,12], functionalized silicas [13,14], metal organic frameworks (MOFs) [15,16], covalent organic frameworks (COFs) [17,18], and molecular organic solids [19,20]. A special group of triazine-based microporous covalent organic polymer (TMCOP) materials developed recently have attracted much interest because these materials have shown promising gas adsorption performances and superb chemical robustness and thermal stability [21–28]. However, most TMCOPs are synthesized under harsh reaction conditions such as high temperature above 673 K and high pressure [21–24]. Herein, we report the synthesis of a novel TMCOP from cyanuric chloride and triphenylamine in the presence of the Lewis acid $AlCl_3$. A similar TMCOP made from the same starting materials has been reported by Xiong and coworkers [29]. However, their synthesis required a strong acid, CH_3SO_3H, in large excess (14 times excess), which requires careful handling. Our synthetic conditions are much milder, the synthetic procedure is facile and easy to scale-up, and more importantly, our product has a larger surface area, enhanced gas selectivity and superb chemical and thermal robustness.

2. Experimental section

2.1. Materials

Cyanuric chloride (99%), triphenylamine (Reagent Plus, 99%), *o*-dichlorobenzene (DCB; anhydrous, 99%), anhydrous aluminum chloride ($AlCl_3$) and hydrochloric acid (HCl) were all purchased

* Corresponding author.
E-mail address: zhiping.lai@kaust.edu.sa (Z. Lai).

http://dx.doi.org/10.1016/j.micromeso.2017.07.038
1387-1811/

from Sigma-Aldrich. Solvents such as tetrahydrofuran (THF), 1,4-dioxane, chloroform ($CHCl_3$), ethanol (EtOH), methanol (MeOH) and acetone were also purchased from Sigma-Aldrich. All of the chemicals were used as received without further purification.

2.2. Solvothermal synthesis

In a typical synthetic procedure, anhydrous aluminum chloride (480 mg, 3.0 mmol) was first dissolved in 10 mL of DCB in a flame-dried Schleck tube under sonication. Next, cyanuric chloride (184 mg, 1.0 mmol) was dispersed in 5 mL of degassed DCB through sonication and then added to the first solution. Triphenylamine (245 mg, 1.0 mmol) was quickly dissolved in 5 mL of degassed DCB and added to the first solution in a dropwise fashion using a syringe under vigorous stirring. The mixture was allowed to stir at room temperature for 6 h. The whole process was carried out under an argon environment. The solution was then refluxed at 463 K for 36 h under an argon environment. After cooling to room temperature, the reddish precipitate was collected by filtration, washed sequentially with dry DCB, methanol, ethanol, acetone, THF and dichloromethane, and finally dried in a drying oven. The sample was purified by Soxhlet extraction using methanol and then treated with 1 M HCl-ethanol solution.

2.3. Characterization techniques

Transmission electron microscopy (TEM) images were taken on an FEI Tecnai twin microscope operated at 120 kV. The samples were first ground into a fine powder and dispersed in ethanol. The solvent was evaporated, leaving the sample deposited on a 400-mesh copper TEM grid. Scanning electron microscopy (SEM) images were obtained using an FEI Nova Nano630 SEM and an FEI Helios NanoLab™ 600 DualBeam operated at 10 kV. The Brunauer-Emmett-Teller (BET) specific surface area was measured on an ASAP 2420 system (Micromeritics) using nitrogen at 77 K. Prior to all gas adsorption measurements, the samples were degassed at 453 K for 24 h under high vacuum. The pore size distribution was derived from the adsorption branch using nonlinear density functional theory (NLDFT). The total pore volume was estimated from the amount of nitrogen adsorbed at a relative pressure of 0.99. Single-component CO_2 and N_2 adsorption isotherms were measured on an ASAP 2050 sorption analyzer (Micromeritics). ^{13}C and ^{15}N NMR measurements were performed on a Bruker 400 M MAS system, and adamantine was used as the internal reference. The rotation frequency was set to 5 kHz. Fourier transform infrared spectroscopy (FTIR) was performed on a Nicolet iS10 smart FTIR spectrometer (Thermo Scientific, USA) equipped with a smart OMNI transmission over a range of 4000 cm^{-1} to 400 cm^{-1}. Thermogravimetric analysis (TGA) and differential thermal analysis (DTA) were carried out on a thermal analyzer TG 209 (Netzsch) under N_2 flow (20 mL/min). The binary gas mixture breakthrough experiments were carried out at 298 K. Detailed information on the breakthrough setup, as well as descriptions of the calculation of the Henry selectivity, IAST selectivity and isosteric heat of adsorption (Q_{st}), are all available in our previous publications [30,31].

3. Results and discussion

Scheme 1 illustrates the formation of the TMCOP structure through a possible Friedel-Craft reaction mechanism in presence of a Lewis acid catalyst, $AlCl_3$ [32,33]. Briefly, $AlCl_3$ first interacts with cyanuric chloride to generate a carbocation complex. Then, the

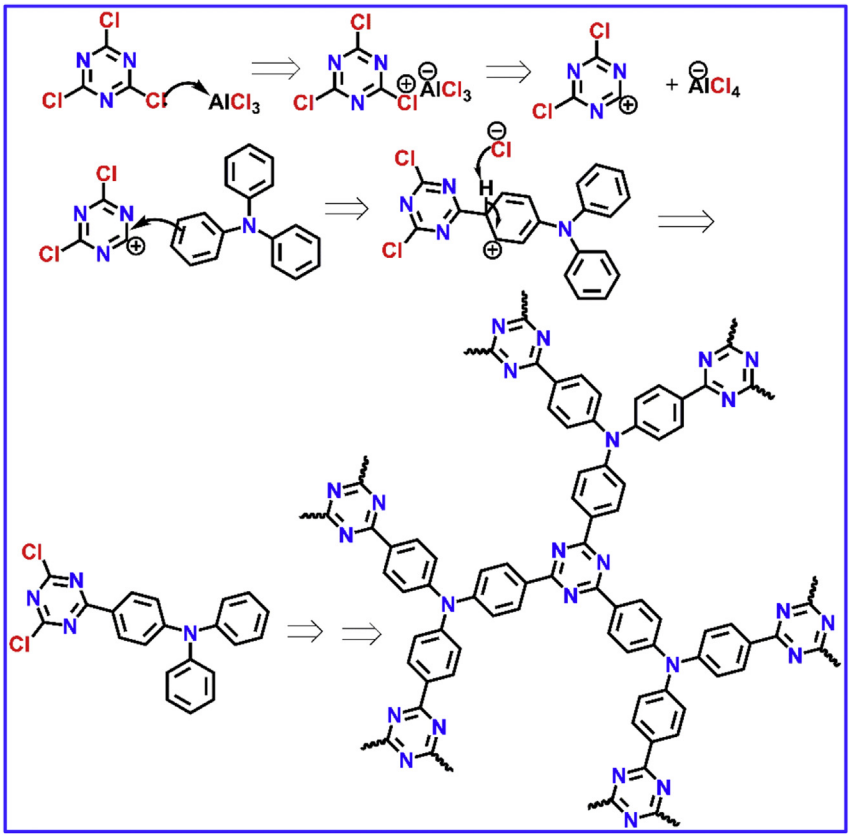

Scheme 1. Schematic representation of the redox mechanism for the formation of TMCOP through a polymerization reaction in the presence of a Lewis acid catalyst, $AlCl_3$.

triphenylamine ligand attacks the carbocation. The product becomes more nucleophilic and hence leads to a subsequent polymerization process to generate the porous polymeric network. The fast reaction rate and non-rigid network allows the system to be controlled kinetically instead of thermodynamically, which favors a highly porous but amorphous structure [21,34]. The covalent bonding and the triazine groups offer high thermal and chemical robustness to the network, while the high density of nitrogen Lewis base favors the adsorption of CO_2, which provides high CO_2 uptake, as well as high selectivity.

The morphology and microstructure of the TMCOP powder are shown in the SEM and TEM images in Fig. 1. Fig. 1a and b shows a spherical morphology with relatively uniform sizes of approximately 1.0–2.0 μm. In the high-resolution TEM images (Fig. 1c), low electron density spots (pores) were observed throughout the specimen with an average size of approximately < 1.0 nm, which was further validated by the NLDFT pore size distribution obtained from the nitrogen sorption analysis (inset of Fig. 2A). The wide-angle powder X-ray diffraction confirmed the typical amorphous nature of the TMCOP material, as shown in Fig. 1f [30].

The ^{13}C NMR spectrum of the TMCOP material is shown in Fig. 2. The ^{13}C NMR spectral band detected at 164.882 ppm indicates the presence of the aromatic carbons in the triazine moiety of the cyanuric chloride component. All three carbons of the triazine moiety are equivalent in the TMCOP material [7]. The other broad peaks at 130–160 ppm correspond to the aromatic carbons in the benzene rings in the triphenylamine moiety [32]. The broad spectra depicted the overlap of all four types of carbon atoms (all peaks are expected to be very close) shown in the proposed scheme. In addition, the ^{15}N CP-MAS spectrum showed two resonance peaks at −72.50 and −357.657 ppm, indicating that the two types of nitrogen functionalities are present in the TMCOP material. The signal at −72.50 ppm corresponds to the nitrogen in the triazine component, whereas the other signal at −357.657 ppm signifies the presence of the tertiary nitrogen atom in the triphenylamine moiety.

Fig. 3 shows the FTIR spectra of TMCOP, cyanuric chloride and triphenylamine. Several strong vibrational bands were detected in the 1200 to 1550 cm^{-1} region, representing typical stretching modes of CN heterocycles [7,35]. The nodal lines resulting from standing waves were used to detect the quadrant and semicircle vibrations of the heteroaromatic rings. The distinct bands related to the quadrant (1590 cm^{-1}) and semicircle stretching (1490 cm^{-1}) of the triazine ring and the characteristic breathing mode band of the triazine unit at 813 cm^{-1} were observed in the TMCOP spectrum, as detonated by the green dotted line in Fig. 3 [36]. The band at

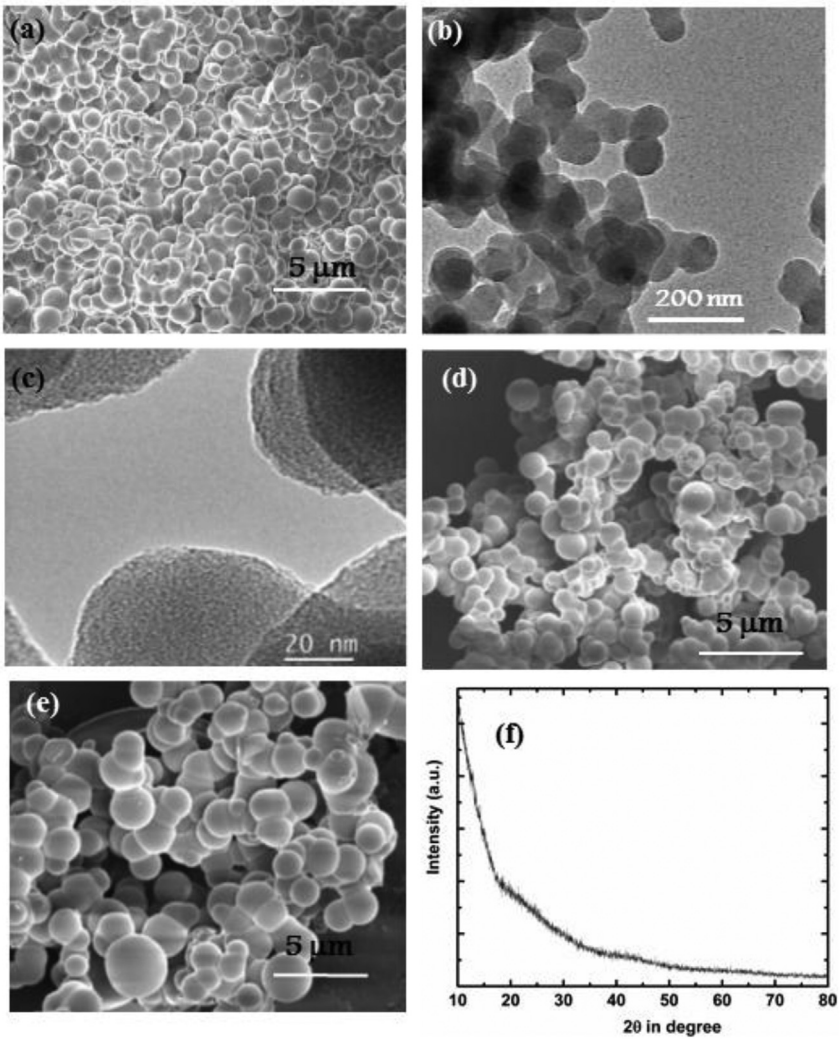

Fig. 1. FE-SEM images of the TMCOP material (a); TEM image at low magnification (b) and HRTEM image (c) at higher magnification of the TMCOP material; FE-SEM images of the TMCOP material after immersion in water for a week (d) and in 0.1 (M) hydrochloric acid in ethanol (e); wide-angle powder X-ray diffraction of the TMCOP material (f).

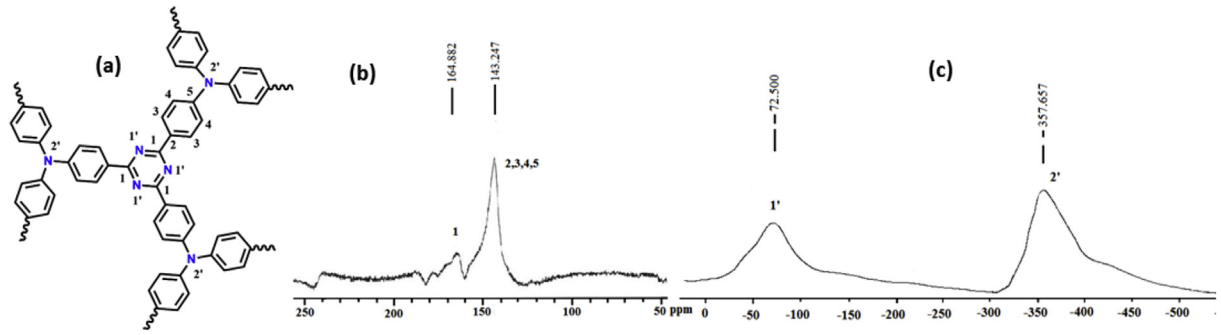

Fig. 2. Schematic representation of the structural bonding in the TMCOP network (a); ^{13}C (b) and ^{15}N (c) solid-state MAS NMR spectra of the porous TMCOP material.

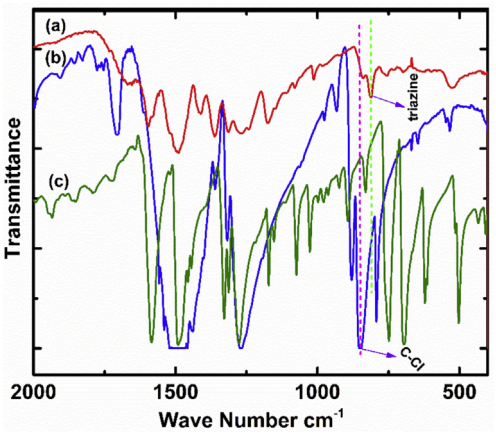

Fig. 3. FTIR spectroscopy of (a) TMCOP, (b) cyanuric chloride and (c) triphenylamine.

760 cm^{-1} corresponding to the bending vibration of C-H in the present 1,4-disubstitued benzene is seen in the spectrum of the presented network [29]. The stretching vibrational bands near 850 cm^{-1} were observed in the cyanuric chloride spectrum as a result of the C-Cl bond, whereas this vibrational band disappeared in the porous TMCOP network, which implies complete substitution of the three chloride atoms in the cyanuric chloride molecule, as marked by the magenta dotted line in Fig. 3, [7,25].

To investigate the thermal stability of the TMCOP material, thermogravimetric analysis of the TMCOP material was carried out up to 1173 K at a ramping rate of 10 K min^{-1} under a continuous N_2 atmosphere, as shown in Fig. 4a. Two sharp drops were observed in the TGA curve. One is before 360 K, which is due to the loss of adsorbed moisture and trapped solvent from the surface and pore interior. The other one is in between 800 and 900 K and is due to the structural decomposition. The experiment demonstrated the high thermal stability of the TMCOP structure, even though it is entirely composed of organic constituents.

The TMCOP material is insoluble in water, and almost all common organic solvents. We further investigated its stability towards humidity, air and/or acid or alkaline media. For example, the material was immersed in water for a week and in 0.1 M HCl or 0.1 M NaOH in ethanol for two days. Then, we investigated the materials by SEM image analyses, and it was observed that the materials retain their spherical microstructure morphology, as shown in Fig. 1d and e.

The nitrogen physisorption isotherm and corresponding pore size distribution of the TMCOP material are shown in Fig. 4b. The obtained isotherm shows a typical type I curve as defined by IUPAC. The observed steep increase in the gas uptake isotherm at low relative pressure (P/P_0) up to 0.09 indicates the presence of a permanent microporosity [37]. The calculated Brunauer-Emmett-Teller (BET) surface area of 1104 m^2g^{-1} is somewhat lower compared to the Langmuir surface area of 1302 m^2g^{-1}. The NLDFT method was used to calculate the pore size distribution, and the majority of the observed pores are micropores approximately

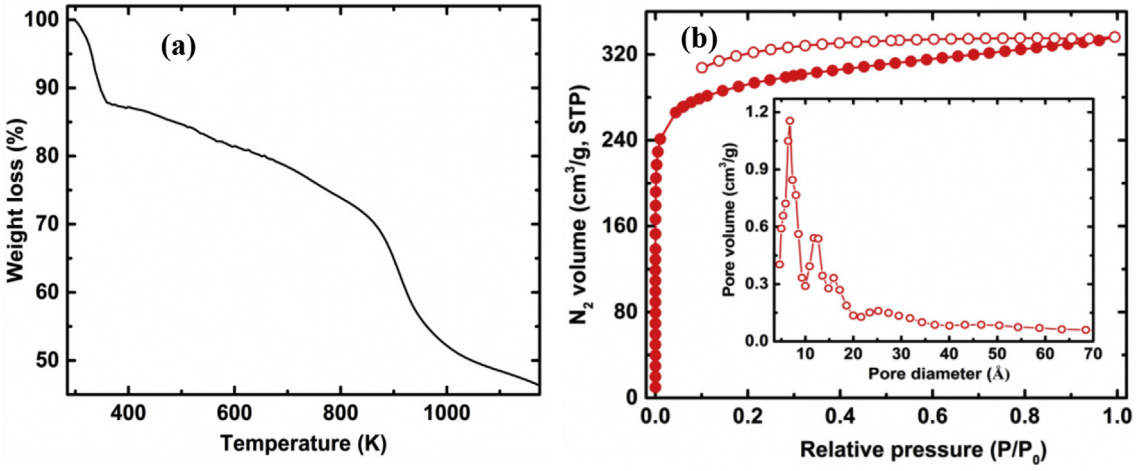

Fig. 4. (a) TGA analysis of the porous TMCOP material and (b) N_2 sorption isotherms of TMCOP measured at 77 K (adsorption: filled circles and desorption: empty circles). The corresponding pore size distribution determined using NLDFT is shown in the inset.

0.65 nm in size. Another peak at 1.19 nm in the supermicropore region was also observed, and this is possibly due to the spatial linkage of the monomers in the polymeric network. No hysteresis loop was observed in the P/P_0 region of 0.40–0.80, confirming the absence of large mesopores. The N_2 sorption isotherm showed that desorption branch does not coincide with the adsorption branch. This may be due to the existence of the narrow micropores that kinetically restrict the exit of adsorbed nitrogen from the pore interior during pressure releasing desorption process [29]. The isotherm is not completely closed at $P/P_0 = 0.20$, which is typical for microporous materials [10,38]. Referring to the results reported by Xiong et al. [29], the reported BET surface is in the range of 428–894 m^2g^{-1}, and the pore size distribution widely spreads from 5 Å to 30 Å. Thus, our sample has a much higher BET surface area and a more uniform pore size distribution.

The single-component adsorption isotherms for CO_2 and N_2 at different temperatures and 1 bar pressure and the corresponding selectivities are shown in Fig. 5a-b. In the studied pressure range, the CO_2 uptake increases with increased pressure and does not reach equilibrium or a saturated state [4,7]. The CO_2 uptake at 1 bar is approximately 3.12 and 1.54 mmol/g at 273 K and 298 K, respectively, whereas the N_2 uptake at 1 bar is approximately 0.20 and 0.12 mmol/g at 273 K and 298 K, respectively. The CO_2/N_2 selectivity in the low-pressure range (<0.1 bar) was estimated using Henry's law [30,39]. The calculated Henry selectivity at 273 K is 64, whereas at 298 K, it is 48, estimated from the linear plot of CO_2 and N_2 uptake at 273 K and 298 K, respectively. Compared to the results reported by Xiong et al., where the CO_2 uptake is around 1.31–2.50 mmol/g at 273 K and 0.78–1.40 mmol/g at 298 K and the CO_2/N_2 selectivity is approximately 27.1–33.7 at 273 K and 25.6–38.7 at 298 K [29], both the CO_2 uptake and CO_2/N_2 selectivity are significantly improved by our new synthetic method. The IAST method was further used to calculate the selectivity of CO_2 over N_2 at 10:90 and 15:85 feed molar compositions (model flue gas composition) [7,40]. The obtained results are given in Fig. 5b, which shows that the selectivity of TMCOP increases with the total feed pressure at a given temperature, while it decreases with increasing temperature at a given feed pressure [41]. For example, at temperature of 273 K and CO_2 to N_2 molar composition of 15:85, the IAST selectivity of CO_2 to N_2 increases from 34 to 46 when total pressure increases from 0.2 to 1 bar, while if the total pressure is fixed at 1 bar, the estimated IAST selectivity (CO_2: N_2 15:85) decreases from 46 to 25 when temperature increases from 273 K to 298 K. The reason for this trend is because that at low pressure most

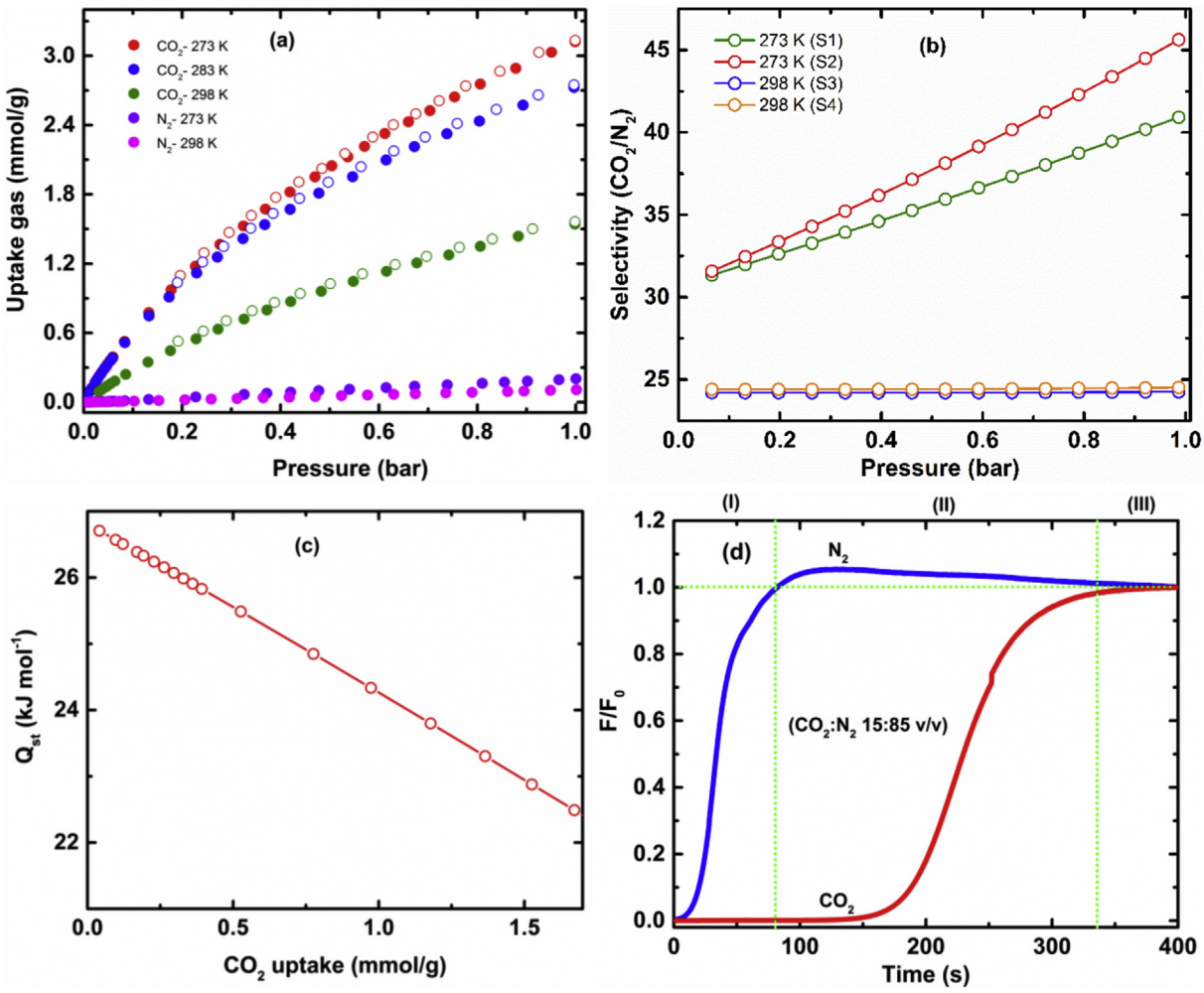

Fig. 5. (a) CO_2 and N_2 sorption isotherms for TMCOP at 273 K, 285 K and 298 K at 1 bar; (b) CO_2/N_2 selectivity of TMCOP using the IAST method with a model flue gas in different composition of CO_2:N_2; 10:90 (S1), 15:85 (S2) at 273 K, and 10:90 (S3), 15:85 (S4) 298 K at 1 bar; (c) isosteric heat of adsorption of TMCOP at different CO_2 uptake [N.B: The isosteric heat of adsorption is negative.]; (d) column breakthrough experimental results for the TMCOP material using a CO_2 and N_2 gas mixture in a model flue gas feed composition of CO_2:N_2 (15:85 v/v) measured at 298 K and 1 bar pressure after activation by continuous He flow at 473 K for 12 h.

Table 1
Comparison of CO_2 and N_2 uptake and CO_2/N_2 separation selectivity of reported porous covalent triazine-based polymers with the synthesized TMCOP material.

Material	CO_2 uptake (mmol/g)		N_2 uptake (mmol/g)		CO_2/N_2 selectivity		Q_{st} of CO_2 (kJ mol^{-1})	Reference
	273 K	298 K	273 K	298 K	273 K	298K		
CTF-1	2.47	1.41	–	–	20	–	27.5	[24]
MCTP-1	4.64	3.08	–	–	–	15	32	[50]
CTP-4	–	2.27	–	–	–	20	33	[32]
NOP-1	2.50	1.40	0.09	–	25.6	–	33.8	[51]
PPF-3	2.09	–	–	–	20		21.8	[42]
PAF-26-COOH	2.32	1.43	0.18	0.14	–	20	28.1	[52]
NPOF-1	2.84	1.52	0.29	0.22	–	8	21.7	[53]
NPOF-1-NO_2	3.97	2.52	0.31	0.23	–	20	29.2	[53]
PAF-5	–	0.27	–	–	–	9.3	26	[54]
TMCOP	3.12	1.54	0.20	0.12	45.6	24.5	26.7	This work

adsorption sites are unsaturated, so the IAST selectivity is close to the single component Henry selectivity; with rising feed pressure and loading, the competition for adsorption sites between CO_2 and N_2 intensifies; therefore the IAST adsorption selectivity rises due to the much higher affinity of CO_2 to the network. Similar observation was also reported in the literature [30,41]. When temperature increases (such as 298 K), the interaction of CO_2 to the network becomes weaker and therefore the selectivity will decrease at a given feed pressure compare to the 273 K, as shown in Fig. 5b. The isosteric heat of adsorption Q_{st} for CO_2 is shown in Fig. 5c. The Q_{st} value calculated in the low uptake range (i.e., low-pressure range) represents the interaction strength between the gas and the adsorbent, i.e., the TMCOP network, whereas at higher loadings, it represents the interactions between the gas molecules. At low loading, the estimated Q_{st} value for CO_2 is 26.7 kJ mol^{-1}. The estimated Q_{st} value for CO_2 of the studied TMCOP material was compared with those of interesting materials reported in the literature; the reported materials listed in Table 1 include PPF-3 (19.4 kJ mol^{-1}) [42], PECONF-1 to PECONF-3 (22.2–24.9 kJ mol^{-1}) [10], BILP-2 (18.4 kJ mol^{-1}), CTPP (34 kJ mol^{-1}) [7], Azo-POF-1 to Azo-POF-2 (26.6–27.5 kJ mol^{-1}) [39], Ene-POF-1 to Ene-POF-2 (24.5–24.6 kJ mol^{-1}) [39] and NOP-19 to NOP-21 (28–37 kJ mol^{-1}). Recently, by incorporating different functional groups (such as $EtNH_2$ or alkynes), modified COF adsorbents showed Q_{st} values ranging from 15.3 to 20.9 kJ mol^{-1} [43], and for other classes of functional materials, CMP-1-COOH = 33 kJ mol^{-1} and BILPs = 26.7–28.8 kJ mol^{-1}. The triazine-based frameworks with enriched Lewis base functionality intrinsically favor interactions with CO_2 over those with N_2. In fact, both CO_2 and N_2 are apolar molecules with similar kinetic diameters, typically 0.34 nm and 0.364 nm, respectively, [16,44,45]. Moreover, the quadrupole moment of CO_2 is 2.85 times larger, and its polarizability is 1.5 times more than that of N_2 [37,45]. All of these differences lead to CO_2 interacting more favorably than N_2 with the Lewis base-enriched TMCOP [46–48], consequently leading to high CO_2 uptake through the dipole and quadrupole interactions of CO_2 molecules.

To demonstrate the effectiveness of the TMCOP material in real applications, we performed breakthrough experiments at ambient pressure and temperature (1 bar; 298 K) under kinetic flow conditions with a model flue gas mixture (15:85 v/v), as shown in Fig. 5d [7,40]. The obtained breakthrough curves can be split into three phases based on the adsorption characteristics [49]. In phase I, the unsaturated TMCOP adsorbent simultaneously captured both CO_2 and N_2 from the mixed gas feed stream. In phase II, the TMCOP continuously uptakes CO_2; however, no additional N_2 was captured, as the adsorbent was saturated with N_2 in phase I. Moreover, in this phase, the TMCOP adsorbent may competitively and/or preferentially uptake CO_2 while a portion of the N_2 (that was adsorbed in the previous phase I) desorbs into the release gas flow. This is the reason why extra N_2 molecules are present in the release stream in phase II. This observation suggested that the TMCOP material can selectively capture CO_2 over N_2 from a mixed gas feed stream. In phase III, the flow rate and composition of the release stream are the same as that of the feed stream because TMCOP was already saturated with both gases from the prior phases. The estimated adsorption capacities for CO_2 and N_2 are 0.70 mmol/g and 0.068 mmol/g, respectively, which translates to a high CO_2/N_2 selectivity of 58.2. The calculated CO_2/N_2 selectivity is very close to the IAST selectivity. The regeneration characteristics of the TMCOP material were also tested in breakthrough experiments by regenerating the material under relatively mild conditions with helium purging (5 mL/min, 353 K for 0.5 h). The regenerated material exhibits adsorption capacities similar to the CO_2/N_2 selectivity observed in the repeated breakthrough experiments.

The comparison of the performance of the studied TMCOP material in the breakthrough selectivity of CO_2/N_2 with the different reported interesting materials is addressed here. Well-known amorphous materials, such as activated carbon and metal-anchored activated carbon (KNC-A-K), resulted in CO_2/N_2 selectivities of 4.5 and 44, respectively [55], as calculated from breakthrough experiments with a 10:90 v/v feed composition of CO_2/N_2 at 298 K and 1 bar. The porous covalent triazine-based materials CTF-1 and fluorinated FCTF-1 exhibited breakthrough selectivities of 18 and 77, respectively [47], and MOFs, such as SIFSIX-2-Cu-I, exhibited a breakthrough selectivity of 72 [56]. Functional metal-doped materials such as Ni/DOBDC (Ni-MOF-74 or CPO-27-Ni) showed flue gas breakthrough selectivities ranging from 22 to 38 [57]. In view of the above comparisons and progress, the flue gas capture and separation performances of the similar types of triazine-based materials reported in the literature, as given in the comparison in Table 1, demonstrated that the studied TMCOP material has comparable or better performance in some cases.

4. Conclusions

The Lewis base-enriched and electron-rich microporous covalent organic polymer adsorbent demonstrated enhanced CO_2 uptake and high CO_2/N_2 separation, as revealed by both single-component gas adsorption studies and column breakthrough experiments, giving the material potential as an adsorbent for flue gas CO_2 capture. The observed enhanced CO_2 uptake and CO_2/N_2 selectivity is due to quadrupole-dipole interactions between the CO_2 molecules and the Lewis base sites (lone pair of electrons on the electronegative nitrogen functionality). Furthermore, the material offers permanent porosity with high surface area and exhibits superior robustness, chemical durability and thermal durability. Thus, the unique nanostructure and enhanced properties (stability, enhanced flue gas capture and separation) of the TMCOP material

highlight it as a promising adsorbent material for environmental remediation.

Acknowledgements

We gratefully acknowledge financial support from the King Abdullah University of Science and Technology (KAUST), competitive research grant URF/1/1378 and baseline fund BAS/1/1375.

List of parameters/symbols with unit

BET	Brunauer-Emmett-Teller (m^2g^{-1})
(P/P_0)	Relative pressures
Q_{st}	Isosteric heat of adsorption (kJ mol^{-1})
F_i	Influent flow rate of gas (mL/m)
F_e	Effluent flow rate of gas (mL/min)
Q	Absolute adsorption capacity of gas (mmol/g)
α	breakthrough selectivity of gases
Y	Molar fraction of gas in the gas mixture
R	Universal gas constant (8.315 J/mol K)
IAST	Ideal adsorption solution theory
q_{sat}	Saturation adsorption capacity (mmol/g)
q_T	Total amount of adsorption (mmol/g)
M	Molarity (mole/liter)
Kinetic Diameter	(Å)
Dipole moment	(esu cm)
Quadrupole moment	(esu cm^2)
Polarizability	(cm^3)

Appendix A. Supplementary data

Supplementary data related to this article can be found at http://dx.doi.org/10.1016/j.micromeso.2017.07.038.

References

[1] V.J. Fabry, B.A. Seibel, R.A. Feely, J.C. Orr, Impacts of ocean acidification on marine fauna and ecosystem processes, ICES J. Mar. Sci. 65 (2008) 414–432.
[2] H.I. Browman, Applying organized scepticism to ocean acidification research, ICES J. Mar. Sci. 73 (2016) 529–536.
[3] X. Wu, B. Yuan, Z. Bao, S. Deng, Adsorption of carbon dioxide, methane and nitrogen on an ultramicroporous copper metal–organic framework, J. Colloid Interface Sci. 430 (2014) 78–84.
[4] B. Yuan, X. Wu, Y. Chen, J. Huang, H. Luo, S. Deng, Adsorption of CO_2, CH_4, and N_2 on ordered mesoporous carbon: approach for greenhouse gases capture and biogas upgrading, Environ. Sci. Technol. 47 (2013) 5474–5480.
[5] R.T. Watson, D.L. Albritton, Climate Change 2001: Synthesis Report: Third Assessment Report of the Intergovernmental Panel on Climate Change, Cambridge University Press, 2001.
[6] A.L. Chaffee, G.P. Knowles, Z. Liang, J. Zhang, P. Xiao, P.A. Webley, CO_2 capture by adsorption: materials and process development, Int. J. Greenh. Gas. Control 1 (2007) 11–18.
[7] S.K. Das, X. Wang, M.M. Ostwal, Y. Zhao, Y. Han, Z. Lai, Highly stable porous covalent triazine–piperazine linked nanoflower as a feasible adsorbent for flue gas CO_2 capture, Chem. Eng. Sci. 145 (2016) 21–30.
[8] A.I. Cooper, Materials chemistry: cooperative carbon capture, Nature 519 (2015) 294–295.
[9] L.-C. Lin, A.H. Berger, R.L. Martin, J. Kim, J.A. Swisher, K. Jariwala, C.H. Rycroft, A.S. Bhown, M.W. Deem, M. Haranczyk, In silico screening of carbon-capture materials, Nat. Mater 11 (2012) 633–641.
[10] P. Mohanty, L.D. Kull, K. Landskron, Porous covalent electron-rich organo-nitridic frameworks as highly selective sorbents for methane and carbon dioxide, Nat. Commun. 2 (2011) 401.
[11] T.C. Drage, J.M. Blackman, C. Pevida, C.E. Snape, Evaluation of activated carbon adsorbents for CO_2 capture in gasification, Energ fuels.. 23 (2009) 2790–2796.
[12] T. Drage, O. Kozynchenko, C. Pevida, M. Plaza, F. Rubiera, J. Pis, C. Snape, S. Tennison, Developing activated carbon adsorbents for pre-combustion CO_2 capture, Energy Procedia 1 (2009) 599–605.
[13] A. Sayari, Y. Belmabkhout, E. Da'na, CO_2 deactivation of supported amines: does the nature of amine matter? Langmuir 28 (2012) 4241–4247.
[14] Y. Jing, L. Wei, Y. Wang, Y. Yu, Synthesis, characterization and CO_2 capture of mesoporous SBA-15 adsorbents functionalized with melamine-based and acrylate-based amine dendrimers, Microporous Mesoporous Mater 183 (2014) 124–133.
[15] Q. Wang, J. Bai, Z. Lu, Y. Pan, X. You, Finely tuning MOFs towards high-performance post-combustion CO_2 capture materials, Chem. Commun. 52 (2016) 443–452.
[16] K. Sumida, D.L. Rogow, J.A. Mason, T.M. McDonald, E.D. Bloch, Z.R. Herm, T.-H. Bae, J.R. Long, Carbon dioxide capture in metal–organic frameworks, Chem. Rev. 112 (2011) 724–781.
[17] Y. Zeng, R. Zou, Y. Zhao, Covalent organic frameworks for CO_2 capture, Adv. Mater. 28 (2016) 2855–2873.
[18] Y. Liu, D. Liu, Q. Yang, C. Zhong, J. Mi, Comparative study of separation performance of COFs and MOFs for $CH_4/CO_2/H_2$ mixtures, Industrial Eng. Chem. Res. 49 (2010) 2902–2906.
[19] J. Tian, P.K. Thallapally, S.J. Dalgarno, P.B. McGrail, J.L. Atwood, Amorphous molecular organic solids for gas adsorption, Angew. Chem. Int. Ed. 48 (2009) 5492–5495.
[20] P.K. Thallapally, B.P. McGrail, J.L. Atwood, C. Gaeta, C. Tedesco, P. Neri, Carbon dioxide capture in a self-assembled organic nanochannels, Chem. Mater 19 (2007) 3355–3357.
[21] P. Katekomol, J.r.m. Roeser, M. Bojdys, J. Weber, A. Thomas, Covalent triazine frameworks prepared from 1, 3, 5-tricyanobenzene, Chem. Mater 25 (2013) 1542–1548.
[22] P. Kuhn, M. Antonietti, A. Thomas, Porous, covalent triazine-based frameworks prepared by ionothermal synthesis, Angew. Chem. Int. Ed. 47 (2008) 3450–3453.
[23] P. Kuhn, A. Forget, J. Hartmann, A. Thomas, M. Antonietti, Template-Free tuning of nanopores in carbonaceous polymers through ionothermal synthesis, Adv. Mater 21 (2009) 897–901.
[24] Y. Zhao, K.X. Yao, B. Teng, T. Zhang, Y. Han, A perfluorinated covalent triazine-based framework for highly selective and water-tolerant CO_2 capture, Energy Environ. Sci. 6 (2013) 3684–3692.
[25] H.A. Patel, F. Karadas, A. Canlier, J. Park, E. Deniz, Y. Jung, M. Atilhan, C.T. Yavuz, High capacity carbon dioxide adsorption by inexpensive covalent organic polymers, J. Mater. Chem. 22 (2012) 8431–8437.
[26] H. Zhao, Z. Jin, H. Su, X. Jing, F. Sun, G. Zhu, Targeted synthesis of a 2D ordered porous organic framework for drug release, Chem. Commun. 47 (2011) 6389–6391.
[27] P. Puthiaraj, S.-M. Cho, Y.-R. Lee, W.-S. Ahn, Microporous covalent triazine polymers: efficient Friedel-Crafts synthesis and adsorption/storage of CO_2 and CH_4, J. Mater. Chem. A 3 (2015) 6792–6797.
[28] Z. Liang, B. Fadhel, C.J. Schneider, A.L. Chaffee, Stepwise growth of melamine-based dendrimers into mesopores and their CO_2 adsorption properties, Microporous Mesoporous Mater 111 (2008) 536–543.
[29] S. Xiong, X. Fu, L. Xiang, G. Yu, J. Guan, Z. Wang, Y. Du, X. Xiong, C. Pan, Liquid acid-catalysed fabrication of nanoporous 1, 3, 5-triazine frameworks with efficient and selective CO_2 uptake, Polym. Chem.-Uk 5 (2014) 3424–3431.
[30] S.K. Das, X. Wang, M.M. Ostwal, Z. Lai, A highly stable microporous covalent imine network adsorbent for natural gas upgrading and flue gas CO_2 capture, Sep. Purif. Technol. 170 (2016) 68–77.
[31] S.K. Das, X. Wang, M.M. Ostwal, Y. Zhao, Y. Han, Z. Lai, Highly stable porous covalent triazine-piperazine linked nanoflower as a feasible adsorbent for flue gas CO_2 capture, Chem. Eng. Sci. (2016), http://dx.doi.org/10.1016/j.ces.2016.1002.1007.
[32] H. Lim, M.C. Cha, J.Y. Chang, Preparation of microporous polymers based on 1, 3, 5-triazine units showing high CO_2 adsorption capacity, Macromol. Chem. Phys. 213 (2012) 1385–1390.
[33] S.K. Das, M.K. Bhunia, A. Bhaumik, Direct synthesis of 2D-hexagonal mesoporous iron silicate and its catalytic activity for selective friedel-crafts alkylation, Open Catal. J. 5 (2012).
[34] P. Kuhn, A. Forget, D. Su, A. Thomas, M. Antonietti, From microporous regular frameworks to mesoporous materials with ultrahigh surface area: dynamic reorganization of porous polymer networks, J. Am. Chem. Soc. 130 (2008) 13333–13337.
[35] K. Kailasam, J. Schmidt, H. Bildirir, G. Zhang, S. Blechert, X. Wang, A. Thomas, Room temperature synthesis of heptazine-based microporous polymer networks as photocatalysts for hydrogen evolution, Macromol. Rapid Commun. 34 (2013) 1008–1013.
[36] M.G. Schwab, B. Fassbender, H.W. Spiess, A. Thomas, X. Feng, K. Mullen, Catalyst-free preparation of melamine-based microporous polymer networks through Schiff base chemistry, J. Am. Chem. Soc. 131 (2009) 7216–7217.
[37] H.A. Patel, F. Karadas, J. Byun, J. Park, E. Deniz, A. Canlier, Y. Jung, M. Atilhan, C.T. Yavuz, Highly stable nanoporous sulfur-bridged covalent organic polymers for carbon dioxide removal, Adv. Funct. Mater 23 (2013) 2270–2276.
[38] O.K. Farha, A.M. Spokoyny, B.G. Hauser, Y.-S. Bae, S.E. Brown, R.Q. Snurr, C.A. Mirkin, J.T. Hupp, Synthesis, properties, and gas separation studies of a robust diimide-based microporous organic polymer, Chem. Mater 21 (2009) 3033–3035.
[39] J. Lu, J. Zhang, Facile synthesis of azo-linked porous organic frameworks via reductive homocoupling for selective CO_2 capture, J. Mater. Chem. A 2 (2014) 13831–13834.
[40] X. Lv, L. Li, S. Tang, C. Wang, X. Zhao, High CO_2/N_2 and CO_2/CH_4 selectivity in a chiral metal–organic framework with contracted pores and multiple functionalities, Chem. Commun. 50 (2014) 6886–6889.
[41] W. Lu, W.M. Verdegaal, J. Yu, P.B. Balbuena, H.-K. Jeong, H.-C. Zhou, Building multiple adsorption sites in porous polymer networks for carbon capture applications, Energy Environ. Sci. 6 (2013) 3559–3564.

[42] Y. Zhu, H. Long, W. Zhang, Imine-linked porous polymer frameworks with high small gas (H_2, CO_2, CH_4, C_2H_2) uptake and CO_2/N_2 selectivity, Chem. Mater 25 (2013) 1630–1635.
[43] N. Huang, R. Krishna, D. Jiang, Tailor-made pore surface engineering in covalent organic frameworks: systematic functionalization for performance screening, J. Am. Chem. Soc. 137 (2015) 7079–7082.
[44] J.A. Mason, T.M. McDonald, T.-H. Bae, J.E. Bachman, K. Sumida, J.J. Dutton, S.S. Kaye, J.R. Long, Application of a high-throughput analyzer in evaluating solid adsorbents for post-combustion carbon capture via multicomponent adsorption of CO_2, N_2, and H_2O, J. Am. Chem. Soc. 137 (2015) 4787–4803.
[45] T.M. McDonald, W.R. Lee, J.A. Mason, B.M. Wiers, C.S. Hong, J.R. Long, Capture of carbon dioxide from air and flue gas in the alkylamine-appended metal–organic framework mmen-Mg_2(dobpdc), J. Am. Chem. Soc. 134 (2012) 7056–7065.
[46] Y. Liu, S. Wu, G. Wang, G. Yu, J. Guan, C. Pan, Z. Wang, Control of porosity of novel carbazole-modified polytriazine frameworks for highly selective separation of CO_2–N_2, J. Mater. Chem. A 2 (2014) 7795–7801.
[47] Y. Zhao, K.X. Yao, B. Teng, T. Zhang, Y. Han, A perfluorinated covalent triazine-based framework for highly selective and water–tolerant CO_2 capture, Energy Environ. Sci. 6 (2013) 3684–3692.
[48] H.A. Patel, S.H. Je, J. Park, D.P. Chen, Y. Jung, C.T. Yavuz, A. Coskun, Unprecedented high-temperature CO_2 selectivity in N_2-phobic nanoporous covalent organic polymers, Nat. Commun. 4 (2013) 1357.
[49] D. Qian, C. Lei, G.-P. Hao, W.-C. Li, A.-H. Lu, Synthesis of hierarchical porous carbon monoliths with incorporated metal–organic frameworks for enhancing volumetric based CO_2 capture capability, ACS Appl. Mater. Inter 4 (2012) 6125–6132.
[50] P. Puthiaraj, S.-M. Cho, Y.-R. Lee, W.-S. Ahn, Microporous covalent triazine polymers: efficient Friedel–Crafts synthesis and adsorption/storage of CO_2 and CH_4, J. Mater. Chem. A 3 (2015) 6792–6797.
[51] S. Xiong, X. Fu, L. Xiang, G. Yu, J. Guan, Z. Wang, Y. Du, X. Xiong, C. Pan, Liquid acid-catalysed fabrication of nanoporous 1,3,5-triazine frameworks with efficient and selective CO_2 uptake, Polym. Chem-Uk 5 (2014) 3424–3431.
[52] H. Ma, H. Ren, X. Zou, S. Meng, F. Sun, G. Zhu, Post-metalation of porous aromatic frameworks for highly efficient carbon capture from CO_2+ N_2 and CH_4+ N_2 mixtures, Polym. Chem.-Uk 5 (2014) 144–152.
[53] T. Islamoglu, T.H. Kim, Z. Kahveci, O.M. El-Kadri, H.M. El-Kaderi, Systematic postsynthetic modification of nanoporous organic frameworks for enhanced CO_2 capture from flue gas and landfill gas, J. Phys. Chem. C 120 (2016) 2592–2599.
[54] S. Sung, M.P. Suh, Highly efficient carbon dioxide capture with a porous organic polymer impregnated with polyethylenimine, J. Mater. Chem. A 2 (2014) 13245–13249.
[55] Y. Zhao, X. Liu, K.X. Yao, L. Zhao, Y. Han, Superior capture of CO_2 achieved by introducing extra-framework cations into N-doped microporous carbon, Chem. Mater 24 (2012) 4725–4734.
[56] P. Nugent, Y. Belmabkhout, S.D. Burd, A.J. Cairns, R. Luebke, K. Forrest, T. Pham, S. Ma, B. Space, L. Wojtas, Porous materials with optimal adsorption thermodynamics and kinetics for CO_2 separation, Nature 495 (2013) 80–84.
[57] J. Liu, J. Tian, P.K. Thallapally, B.P. McGrail, Selective CO_2 capture from flue gas using metal-organic frameworks-a fixed bed study, J. Phys. Chem. C 116 (2012) 9575–9581.